Journal of Reproduction and Development, Vol. 61, No 5, 2015

—Original Article—

Distribution of the sex chromosome during mouse spermatogenesis in testis tissue sections

Kosuke OTAKA[1)], Yuuki HIRADATE[1)], Norio KOBAYASHI[1)], Yoshiki SHIRAKATA[1)] and Kentaro TANEMURA[1)]

[1)]*Laboratory of Animal Reproduction and Development, Graduate School of Agricultural Science, Tohoku University, Miyagi 981-8555, Japan*

Abstract. During mammalian spermatogenesis, spermatogenic cells undergo mitotic division and are subsequently divided into haploid spermatids by meiotic division, but the dynamics of sex chromosomes during spermatogenesis are unclear *in vivo*. To gain insight into the distribution of sex chromosomes in the testis, we examined the localization of sex chromosomes before and after meiosis in mouse testis sections. Here, we developed a method of fluorescence *in situ* hybridization (FISH) using specific probes for the X and Y chromosomes to obtain their positional information in histological testis sections. FISH analysis revealed the sex chromosomal position during spermatogenesis in each stage of seminiferous epithelia and in each spermatogenic cell. In the spermatogonia and leptotene spermatocytes, sex chromosomes were distantly positioned in the cell. In the zygotene and pachytene spermatocytes at prophase I, X and Y chromosomes had a random distribution. After meiosis, the X and Y spermatids were random in every seminiferous epithelium. We also detected aneuploidy of sex chromosomes in spermatogenic cells using our developed FISH analysis. Our results provide further insight into the distribution of sex chromosomes during spermatogenesis, which could help to elucidate a specific difference between X and Y spermatids and sex chromosome-specific behavior.

Key words: Fluorescence *in situ* hybridization, Sex chromosome, Spermatogenesis

(**J. Reprod. Dev. 61:** 375–381, 2015)

In the process of mammalian spermatogenesis, diploid spermatogonia finally divide into haploid spermatids that bear either the X or Y chromosome through mitotic and meiotic divisions. A previous study focusing on the behavior of sex chromosomes in cells undergoing spermatogenesis indicated that the pairing patterns of autosomes and sex chromosomes are different [1]. Autosomes undergo pairing over the entire length of the homologs in both meiosis and mitosis, whereas sex chromosomes form a synapsis at the pseudoautosomal region in the first meiotic division [2–4]. In early pachytene spermatocytes, sex chromosomes form a condensed chromatin domain termed the sex body or XY body [1, 2, 5, 6]. Furthermore, the sex chromosome is transcriptionally silenced in late pachytene spermatocytes; this phenomenon is known as meiotic sex chromosome inactivation (MSCI) [7–11]. Failure of the pairing synapsis or MSCI causes apoptosis at pachytene of the seminiferous epithelium at pachytene stage IV [12–14].

Whereas these studies focused on the sex chromosome-specific behavior in spermatocytes up to the pachytene stage, recent studies have revealed the distribution of sex chromosomes in meiotic prophase [6], before and after meiotic division [15] and in spermatozoa and embryos [16] by fluorescence *in situ* hybridization (FISH). In addition, FISH analysis to detect sex chromosomes for sexing and detecting aneuploidy in spermatozoa has been used in several mammalian species such as the mouse [16, 17], human [18–20], canine [21, 22], swine [23], bovine [24–27], and stallion [28]. However, previous studies used isolated spermatogenic cells or focused on spermatozoa; the distribution and aneuploidy of sex chromosomes have not been investigated during spermatogenesis *in vivo*. FISH using tissue sections can indicate the localization of the sex chromosome at each differentiation stage of spermatogenic cells. Therefore, we developed a FISH method using mouse testis tissue sections to determine the localization of the sex chromosome.

In the mouse testis, spermatogenesis occurs within seminiferous tubules, where spermatogenic cells differentiate successively. The differentiation stages of spermatogenesis can be divided mainly into three cell types according to cell maturation: spermatogonia, spermatocytes and spermatids [29]. Spermatogonia undergo mitotic division and subsequently become immature primary spermatocytes termed preleptotene spermatocytes. Spermatocyte development comprises the preleptotene, leptotene, zygotene, pachytene and diplotene stages. One spermatocyte finally differentiates into four spermatids that bear either an X or a Y chromosome through meiotic division. Differentiation stages of spermatids are categorized into steps 1–16. The spermatids of steps 1–8 are circular and are termed round spermatids. Spermatids after step 8 are termed elongated spermatids, and they mature into sperm after spermiogenesis [30]. A cross section of the seminiferous epithelium shows a specific constitution of spermatogenic cells [30]. In mice, spermatogenesis

Received: February 9, 2015
Accepted: May 6, 2015
Published online in J-STAGE: June 14, 2015

Correspondence: K Tanemura (e-mail: kentaro@m.tohoku.ac.jp)

occurs within seminiferous tubules and can be classified into 12 different stages according to the composition of maturing spermatogenic cells [30, 31]. A section of seminiferous epithelium contains cells in three to four different maturation steps; for example, the stage VIII seminiferous epithelium contains preleptotene spermatocytes, pachytene spermatocytes, step 8 round spermatids and step 16 elongated spermatids [30, 31]. Thus, it is possible to simultaneously obtain the positional information of sex chromosomes and cell type in each stage of spermatogenesis.

However, it is difficult to detect FISH signals in tissue sections. In elongated spermatids in particular, most histone proteins are substituted with protamines and the chromatin is tightly packed. As such, compaction probably prevents the hybridization of probes. As a result, a decondensation treatment step, such as incubation with proteinase K, is required to detect the sex chromosome signals in elongated spermatids. In this study, we successfully detected the sex chromosome signals in paraffin-embedded methacarn-fixed testicular tissue sections using antigen retrieval solution and could obtain positional information on the sex chromosomes.

Material and Methods

Animals

We purchased 8-week-old male C57/BL6 mice from Japan SLC (Shizuoka, Japan). The mice were anesthetized with 2,2,2-tribromoethanol. Their testes were surgically removed, fixed with methacarn fixative (methanol:chloroform:acetic acid = 6:3:1), treated with 100% ethanol and xylene and embedded in paraffin. The care and use of all the mice conformed to the Regulations for Animal Experiments and Related Activities at Tohoku University.

Slide preparation, fixation of mouse testis and FISH

Mouse testes were surgically removed, fixed with methacarn fixative, and embedded in paraffin. Cross sections (10 μm) were deparaffinized with xylene and incubated at 98 C for 50 min with Histo VT One (Nacalai Tesque; Japan, Kyoto). To observe the signals of the elongated spermatids, we incubated the sample in 0.001% proteinase K/phosphate-buffered saline solution at 37 C for 5 min. After washing, sections were dehydrated in 70% and 100% ethanol for 5 min each and air dried. Then, samples were incubated with 10 μl mouse XY chromosome FISH probe (Y: fluorescein isothiocyanate [FITC]; X, biotin; MXY-10, Chromosome Science Labo, Sapporo, Japan). Slides were covered with parafilm and incubated at 90 C for 10 min on a heat plate. After hybridization for 24 h at 37 C in a humid chamber, slides were incubated in 2 × standard saline citrate (SSC, Nacalai Tesque, Kyoto), and then the parafilm was gently removed. Slides were rinsed in 1 × SSC at 37 C for 20 min. Some sections were incubated with Blocking One (Nacalai Tesque) at 4 C for 1 h and then sequentially reacted with Alexa Fluor 555 streptavidin (diluted 1:1,000, S32355, Invitrogen, Waltham, MA, USA), Hoechst 33342 (diluted 1:5,000, Molecular Probes, Eugene, OR, USA), rabbit polyclonal anti-fluorescein/Oregon Green antibody (diluted 1:2,000, A889; Molecular Probes), and Alexa Fluor 488-labeled anti-rabbit (diluted 1:2,000, A11034; Molecular Probes) as a secondary antibody for anti-fluorescein. FISH images were obtained by sequential scanning using an LSM-710 confocal laser microscope (Carl Zeiss, Jena, Germany) and analyzed with the ZEN-2010 software in conjunction with an LSM-700 microscope. The stage of each seminiferous tubule was judged according to the criteria described previously [30].

Signal count and statistical analysis of FISH slides to detect sex chromosome aneuploidy and determine deviation from expected sex ratios

The mean fluorescence intensity of spermatogenic cells was measured with the ZEN-2010 software in conjunction with an LSM-700 microscope. Fluorescence brightness was classified into 255 levels.

To separate the sex chromosome signal from noise, we defined the signal as a fluorescence intensity that was greater than 50 at one or more point-like signals in the nucleus; a fluorescence intensity below 50 was characterized as "without signal". In preleptotene and pachytene spermatocytes in stage VIII seminiferous tubules, if only X or Y was not detected, the spermatocytes were classified as "without signal." to accurately calculate the hybridization efficiency. If step 8 spermatids had two or more signals, the cells were considered to be aneuploid. It was difficult to count the signals of elongated spermatids because many of them overlapped. In this study, therefore, we counted the signals of preleptotene spermatocytes, pachytene spermatocytes, and step 8 spermatids using the FISH method without proteinase K. We chose 12 stage VIII seminiferous tubules in one cross section for analysis. We evaluated aneuploidy as described by Komaki *et al.* [22]. A chi-squared test was used to investigate the deviation from the expected ratio of 50:50 (X:Y). Differences were considered significant at a level of $P < 0.05$.

Results

FISH analysis of sex chromosome distribution during spermatogenesis

We showed the distribution of sex chromosomes in stages I, V, VIII, X and XII seminiferous epithelia (Fig. 1A–X and Fig. 2A–E) and that of step 16 spermatids (Fig. 1a–d and Fig. 2F). The stage of each seminiferous epithelium was classified according to the criteria described previously [30]. At the phase of elongated spermatids, the chromosomes became tightly packed with protamine, a histone-like protein. This condensation of chromatin probably makes it difficult for the probes to hybridize. In the step 13, 15 and 16 spermatids, we were only able to detect the signal of the X chromosome (arrow in Fig. 1D, H, L and P). Therefore, we treated the section with proteinase K to degrade the protamine to detect sex chromosome signals in step 16 spermatids (Fig. 1a–d and Fig. 2F).

During spermatogenesis, the localization of sex chromosomes varied dynamically. In the preleptotene and leptotene stages, sex chromosomes were distantly positioned (star in Fig. 1P and T). However, during the zygotene stage, the signals were closely positioned (asterisk in Fig. 1X). In the pachytene stage, the signals remained close together (asterisk in Fig. 1H, L, P and T). The round spermatids in the seminiferous epithelium of each stage had a random distribution of X- and Y-bearing spermatids (Fig. 1D, H, L, P, T and X and Fig. 2A–D).

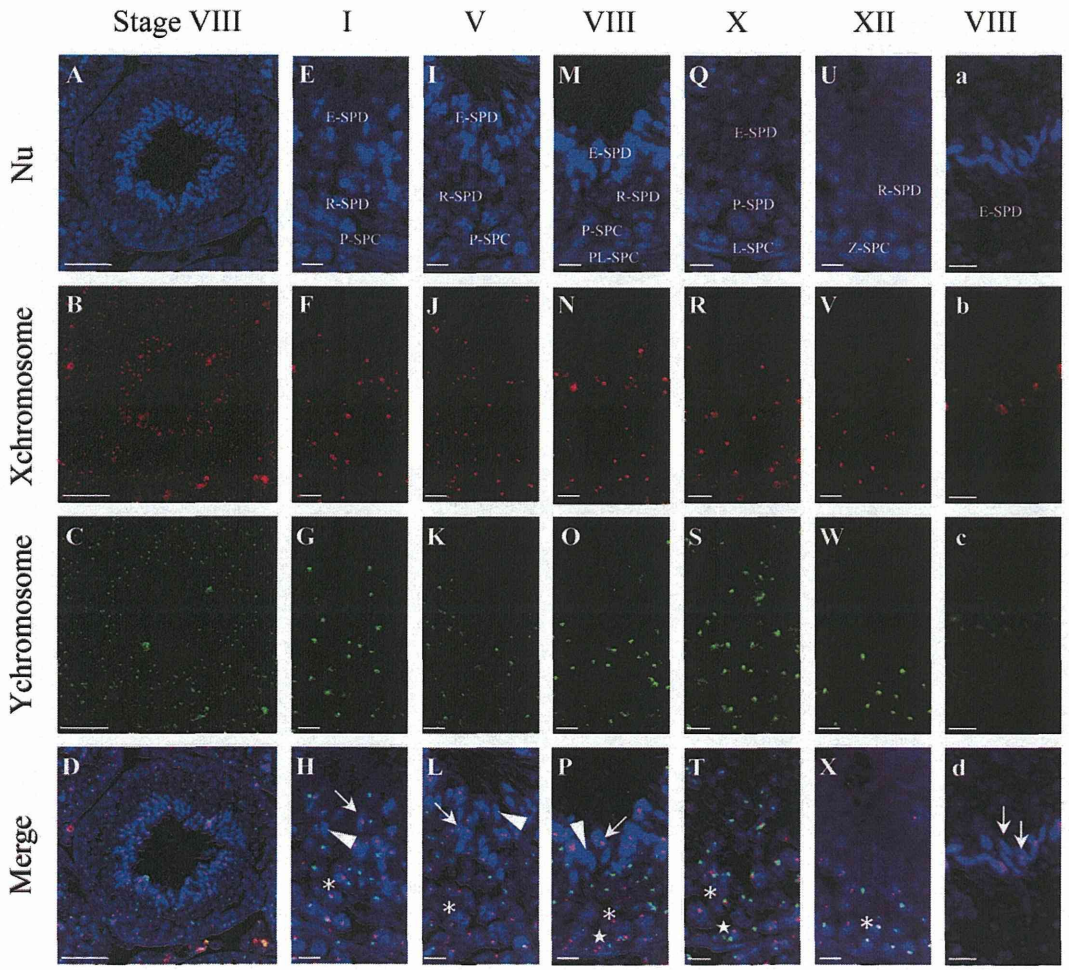

Fig. 1. Fluorescence *in situ* hybridization (FISH) analysis of sex chromosome distribution during spermatogenesis. The signals represent the nucleus (A, E, I, M, Q, U and a), X chromosome (B, F, J, N, R, V and b), and Y chromosome (C, G, K, O, S, W and c). A stage VIII seminiferous tubule is shown (A, B, C, D, a, b, c and d). Stage I (E, F, G and H), stage V (I, J, K and L), stage VIII (M, N, O and P), stage X (Q, R, S and T) and stage XII (U, V, W and X) seminiferous tubules are shown. Cells without proteinase K treatment are shown (A–X). Cells with proteinase K treatment are shown (a–d). Arrowheads, elongated spermatid without signal; long arrows, elongated spermatid with signal. The scale bar represents 50 μm (A, B, C, D) and 10 μm (E–X). P-SPC, pachytene spermatocyte; PL-SPC, preleptotene spermatocyte; L-SPC, leptotene spermatocyte; Z-SPC, zygotene spermatocyte; R-SPD, round spermatid; and E-SPD, elongated.

FISH analysis of sex chromosome localization in each stage of differentiation

FISH revealed the localization of the sex chromosome in each spermatogenic cell differentiation stage (Fig. 3A–M). We determined the sex chromosome localization in spermatogonia, preleptotene spermatocytes, leptotene spermatocytes, zygotene spermatocytes, pachytene spermatocytes, diplotene spermatocytes, during meiosis, round spermatids and elongated spermatids by FISH of mouse testis sections (Fig. 3A–M). The differentiation stages of spermatogenic cells were classified according to the criteria described previously [30]. In spermatogonia, X and Y chromosome signals were distantly positioned (Fig. 3A). Preleptotene spermatocytes and leptotene spermatocytes also had separated X and Y chromosome signals (Fig. 3B and C). In zygotene spermatocytes, the signals were close together (Fig. 3D). In pachytene spermatocytes, these signals were localized along the outer edge of the nucleus and formed a condensed chromatin domain termed the XY body (Fig. 3E) [1, 2, 5, 6]. In diplotene spermatocytes, the signals were similar to those of pachytene spermatocytes, but the signals in diplotene spermatocytes are known to move toward the center of the nucleus (Fig. 3F) [6, 15]. In round spermatids, X and Y chromosomes were individually positioned at the edge of the nucleus (Fig. 3I-a and I-b), and the position did not appear to be different for the X chromosome and Y chromosome in the nucleus. In addition, we detected aneuploidy of sex chromosomes in round spermatids (Fig. 3K, L, and M). In elongated spermatids, the X and Y chromosomes were located in different positions in each cell (Fig. 1d, Fig. 2F and Fig. 3J). These localization patterns are consistent with those of previous studies *in vitro* [6, 8, 15]. We examined the

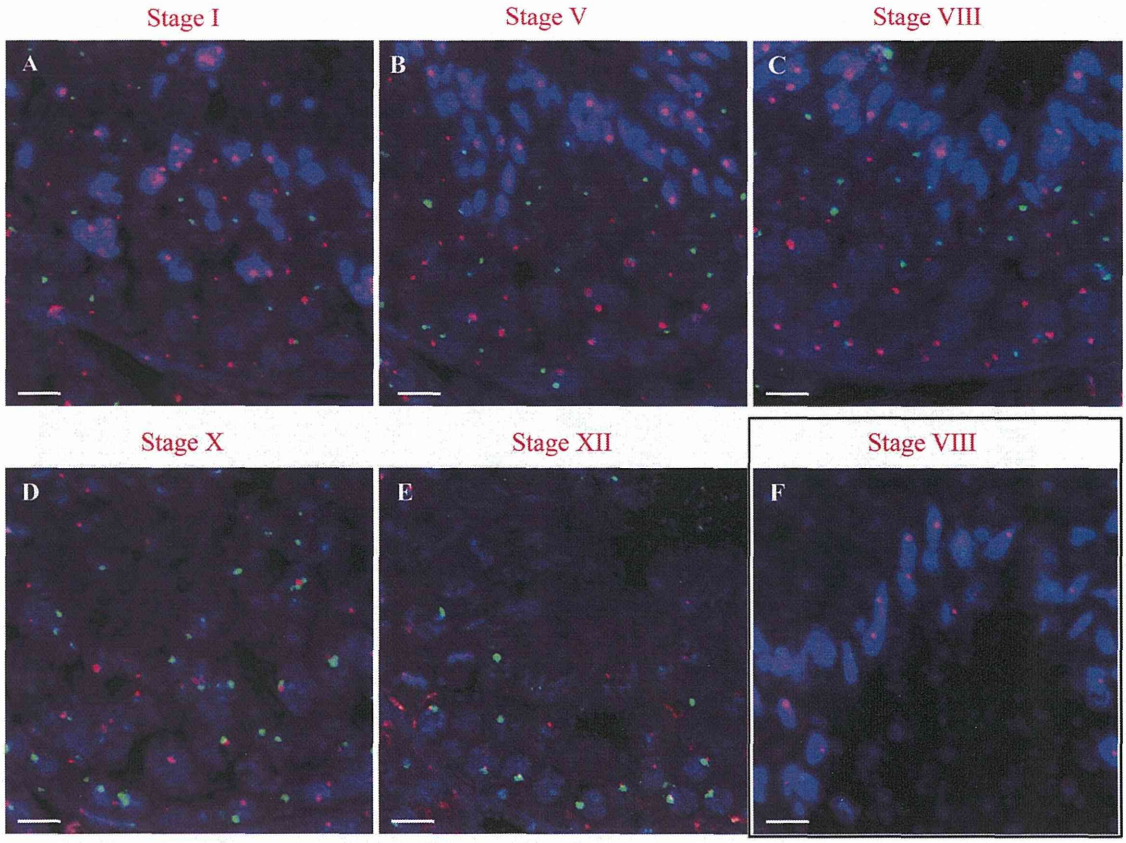

Fig. 2. FISH analysis of sex chromosome distribution in the stage I, V, VIII, X and XII seminiferous epithelium. The signals represent the nucleus (blue), X chromosome (red) and Y chromosome (green). Stage I (A), stage V (B), stage VIII (C, F), stage X (D) and stage XII (E) seminiferous tubules are shown. Cells with proteinase K treatment are surrounded by a frame and shown (F). The scale bar represents 10 μm.

sex chromosome-specific localization before and after meiosis (Fig. 3G-a, G-b, H-a and H-b) in stage XII seminiferous epithelia. At metaphase of the first meiotic division, sex chromosomes overlapped on the metaphase plate (asterisk in Fig. 3G-a). At anaphase of the first meiotic division, sex chromosomes were positioned distantly (Fig. 3G-b). After the second meiotic division, sex chromosomes were individually located in X- or Y-bearing spermatids (Fig. 3H-a and H-b).

Signal counting of the sex chromosomes in stage VIII seminiferous tubules

We counted the X and Y chromosome signals in spermatogenic cells and disomic spermatids in stage VIII seminiferous tubules (Table 1). We observed 12 seminiferous tubules and detected 2,884 specific signals in 3,181 spermatogenic cells. The hybridization efficiency was 91.35 ± 2.42% (Table 1). There was no significant difference between the theoretical ratio (50:50) and the observed ratio of X and Y chromosomes in step 8 spermatids of each stage VIII seminiferous tubule (Table 2). Of the examined spermatids, 45.975 ± 3.570% had an X chromosome signal, whereas 46.742 ± 3.701% had a Y chromosome signal (Table 2). The percentages of XX-, YY- and XY-bearing spermatids were 0.086 ± 0.203%, 0.157 ± 0.285 and 0.403 ± 0.337, respectively. The percentage of spermatids without a sex chromosome signal was 7.195 ± 3.205%. The mean frequency and standard deviation of the percentage of sex chromosome aneuploidy was 0.215 ± 0.068%.

Discussion

In this study, we examined the distribution of sex chromosomes during spermatogenesis and determined their localization in each spermatogenic cell. Previous studies have shown the localization of sex chromosomes in each spermatogenic cell by FISH *in vitro* [6, 15, 16]. However, these studies used isolated cells from the mouse testis, and observation of a series of sex chromosome distributions during spermatogenesis has not been demonstrated. Therefore, we reasoned that use of histological tissue would be a useful approach to obtaining comprehensive information. During spermatogenesis, the position of sex chromosomes changes dynamically [2, 6]. Sex chromosomes become distantly positioned or co-localized during spermatogenesis (Fig. 3A–J). These findings are consistent with those of prior studies *in vitro* [6, 15]. We observed sex chromosome

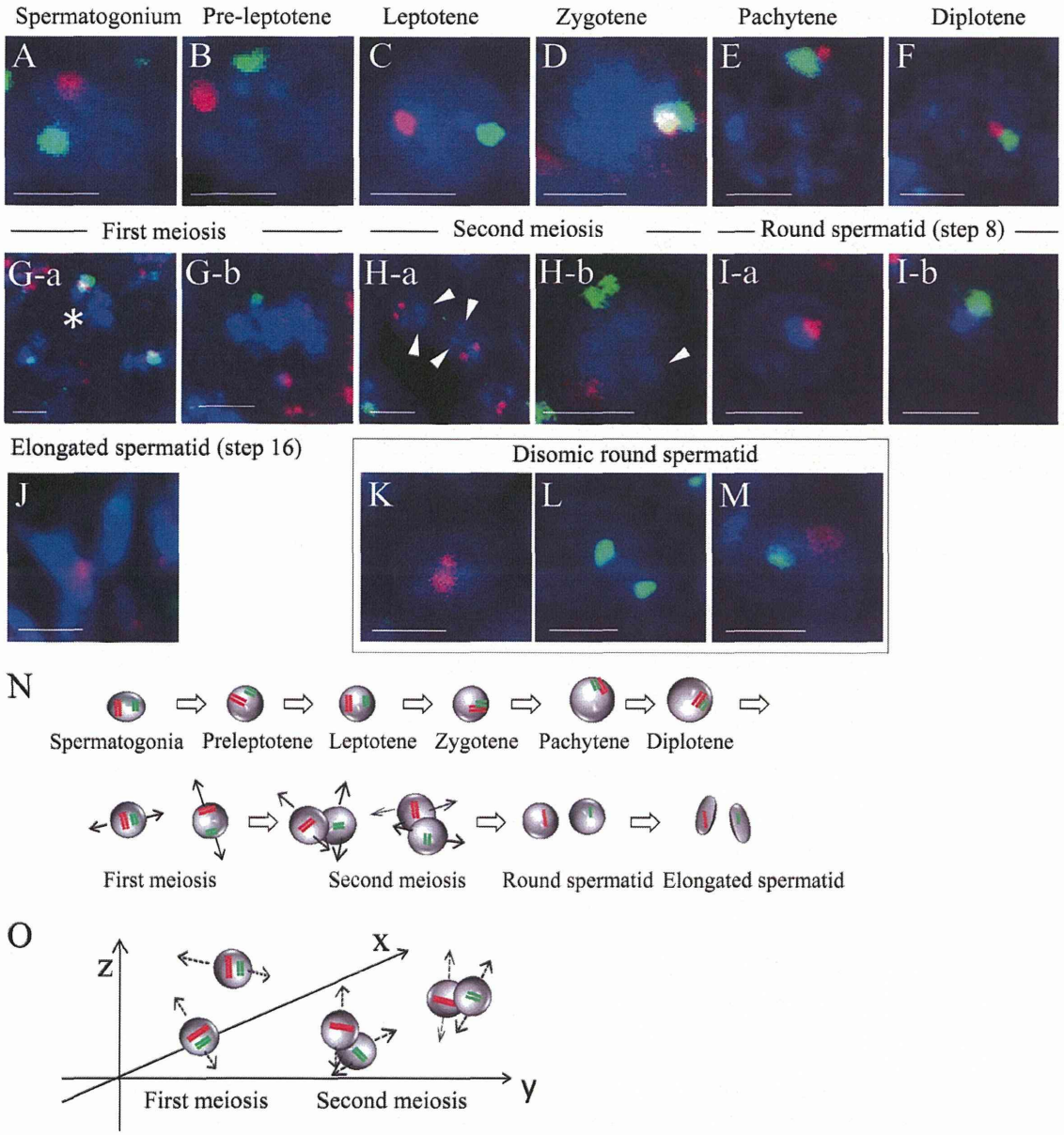

Fig. 3. FISH analysis of sex chromosome localization in each stage of spermatogenic cells. The signals represent the nucleus (blue), X chromosome (red) and Y chromosome (green) (A–O). (A) Spermatognium, (B) preleptotene spermatocyte, (C) leptotene spermatocyte, (D) zygotene spermatocyte, (E) pachytene spermatocyte, (F) diplotene spermatocyte, (G-a, G-b) spermatogenic cells during first meiosis, (H-a, H-b) spermatids after meiosis, (I-a) X spermatid, (I-b) Y spermatid and (J) elongated spermatid. Disomic spermatids are shown (K, L and M): (K) XX spermatid, (L) YY spermatid and (M) XY spermatid. All disomic spermatids were identified in stage VIII seminiferous tubules. Arrowheads show spermatids without a signal. The scale bar represents 5 μm. (N) Schematic of spermatogenesis. Long arrows, direction of meiosis. (O) Scheme of dynamics in meiosis. An arrow with a solid line shows the axis of coordinates, and an arrow with a dotted line shows the direction of meiosis.

position dynamics during meiosis (Fig. 3G-a, G-b, H-a and H-b). Sex chromosome dynamics are less well understood in spermatogenic cells during meiotic division. Figure 3N shows the distribution of sex chromosomes during spermatogenesis according to our results. Our results will facilitate the study of sex chromosome-specific dynamics.

Additionally, FISH revealed the distribution of X- or Y-bearing spermatids after meiotic division in seminiferous epithelium of each stage. They were located at random in the seminiferous epithelium (Fig. 1D, H, L, P and T and Fig. 2A–E), and we did not observe deviation to one side or the other. These findings suggest that every spermatogenic cell after meiotic division may be divided multidirectionally and may not always be pushed out toward the

Table 1. Signal count in stage VIII seminiferous tubules

Stage VIII seminiferous tubule	PL	P	X spermatid	Y spermatid	XX spermatid	YY spermatid	XY spermatid	Total signals	Total without signal	Hybridization efficiency (%)
No. 1	38	56	90	106	0	0	1	291	14	95.41
No. 2	35	30	95	76	0	0	0	236	20	92.19
No. 3	49	62	95	111	0	0	1	318	29	91.64
No. 4	38	74	96	110	1	0	1	320	18	94.67
No. 5	48	54	89	94	0	0	1	286	32	89.94
No. 6	43	53	83	67	0	0	1	247	24	91.14
No. 7	34	65	74	80	0	1	0	254	29	89.75
No. 8	37	60	91	88	0	0	2	278	26	91.45
No. 9	42	70	76	79	1	1	1	270	18	93.75
No. 10	37	47	66	64	0	1	1	216	24	90.00
No. 11	44	22	87	77	0	0	0	230	32	87.79
No. 12	42	58	61	74	0	0	0	235	31	88.35
Mean ± SD										91.34 ± 2.38

PL, preleptotene spermatocyte; P, pachytene spermatocyte.

Table 2. Percentages (%) of X and Y spermatid and sex chromosome aneuploidy in step 8 spermatids

Stage VIII seminiferous tubule	X	Y	XX	YY	XY	Without signal	Total spermatids (N)
No. 1	45.23	53.27	0	0	0.50	1.02	197
No. 2	53.37	42.70	0	0	0	4.09	171
No. 3	41.30	48.26	0	0	0.43	11.11	207
No. 4	43.44	49.77	0.43	0	0.45	6.25	208
No. 5	43.84	46.31	0	0	0.49	10.33	184
No. 6	50.92	41.10	0	0	0.61	7.95	151
No. 7	44.31	47.90	0	0.60	0	7.74	155
No. 8	47.64	46.07	0	0	1.05	5.52	181
No. 9	46.34	48.17	0.60	0.61	0.61	3.80	158
No. 10	44.90	43.54	0	0.68	0.68	11.36	132
No. 11	48.33	42.78	0	0	0	9.76	164
No. 12	42.07	51.03	0	0	0	7.41	135
Mean ± SD	45.97 ± 3.570	46.74 ± 3.701	0.086 ± 0.203	0.157 ± 0.285	0.403 ± 0.337	7.195 ± 3.205	

X, X-bearing spermatid; Y, Y-bearing spermatid; XX, X disomic spermatid; YY, Y disomic spermatid; XY, XY disomic spermatid.

lumen. We speculated that spermatogenic cells divide in multiple directions in seminiferous tubules during meiosis in spermatogenesis. Therefore, we created a model of the multidirectional division (Fig. 3O). There are no reports focusing on the difference in sex chromosome dynamics during cell division between somatic and germ cells. The differences between cells such as somatic cells and oocytes having two X chromosomes and between somatic cells and spermatogenic cells having X and Y chromosomes are interesting. In a recent study, the dynamics of oocytes during meiosis were examined by live-cell imaging [32]. In addition, a protein that controls the first meiotic division pattern was identified in the mouse [33]. However, in spermatogenic cells, the *in vivo* cell division pattern is unclear. Further analysis is needed to understand the division pattern of meiosis of spermatogenic cells *in vivo*.

In this study, we demonstrated a method of detecting sex chromosome signals not only during the round spermatid stage, but also in step 16 elongated spermatids. Our FISH method using tissue sections allowed us to investigate the sex chromosome state corresponding to the cell developmental stage during spermatogenesis. Without proteinase K, X chromosome signals could be detected in step 13, 15 and 16 elongated spermatids (Fig. 1D, H, L and P and Fig. 2C). This was attributed to the different designs of the X and Y probes. The X probe was designed from an approximately 0.5-Mb array near the telomere, whereas the Y probe used a painting probe to detect the signal easily. During spermatogenesis, most histone proteins are exchanged for protamine in elongating spermatids [34]. Therefore, a decondensation process is needed to detect the Y chromosome signals within the nucleus of elongated spermatids [18, 20]. We observed Y chromosome signals in step 16 spermatids after treatment with proteinase K (Fig. 1a–d and Fig. 2F).

FISH revealed sex chromosome aneuploidy in mouse testis sections (Fig. 3K, L and M). The percentages of disomic spermatids were 0.086 ± 0.203% (XX), 0.157 ± 0.285% (YY) and 0.403 ± 0.337% (XY) in step 8 spermatids (Table 2). Although failures of MSCI and

chromosome synapsis cause cell death in pachytene spermatocytes [12–14, 35], disomic sex chromosome spermatids might remain in spermatogenesis. In previous studies, Baumgartner *et al.* showed that the rates of murine disomic spermatozoa were 0.016% (XX), 0.004% (YY), and 0.007% (XY) [36]; Attia *et al.* showed that the values were 0.022% (XX), 0.012% (YY), and 0.002% (XY) [37]; and Attia showed that the values were 0.013% (XX), 0.011% (YY), and 0.004% (XY) [38]. In our study, the rate of murine disomic spermatozoa was relatively high, with values of 0.086 ± 0.203% (XX), 0.157 ± 0.285 (YY) and 0.403 ± 0.337 (XY) in round spermatids. These differences may be because we evaluated round spermatids and disomic sex chromosome spermatids might appear more frequently than disomic spermatozoa. In fact, a recent study demonstrated that the number of aneuploid spermatids was greater than that of spermatozoa in humans [39]. Our method of determining sex chromosomal localization using FISH of testis tissue sections can be applied to further investigations of aneuploidy in each spermatogenic cell in mouse testis sections.

In this study, we developed a FISH method to examine the sex chromosome distribution during murine spermatogenesis using testis tissue sections. Our method enables the detection of X and Y chromosome signals in each spermatogenic cell. These results can provide further insight into the dynamics of sex chromosome localization during spermatogenesis and facilitate the study of specific differences between X and Y spermatids.

References

1. **Handel MA.** The XY body: a specialized meiotic chromatin domain. *Exp Cell Res* 2004; **296**: 57–63.
2. **Solari AJ.** The behavior of the XY pair in mammals. *Int Rev Cytol* 1974; **38**: 273–317.
3. **Burgoyne PS.** Genetic homology and crossing over in the X and Y chromosomes of Mammals. *Hum Genet* 1982; **61**: 85–90.
4. **Kauppi L, Jasin M, Keeney S.** The tricky path to recombining X and Y chromosomes in meiosis. *Ann N Y Acad Sci* 2012; **1267**: 18–23.
5. **McKee BD, Handel MA.** Sex chromosomes, recombination, and chromatin conformation. *Chromosoma* 1993; **102**: 71–80.
6. **Baarends WM, Grootegoed JA.** Chromatin dynamics in the male meiotic prophase. *Cytogenet Genome Res* 2003; **103**: 225–234.
7. **Fernandez-Capetillo O, Mahadevaiah SK, Celeste A, Romanienko PJ, Camerini-Otero RD, Bonner WM, Manova K, Burgoyne P, Nussenzweig A.** H2AX is required for chromatin remodeling and inactivation of sex chromosomes in male mouse meiosis. *Dev Cell* 2003; **4**: 497–508.
8. **Turner JM, Aprelikova O, Xu X, Wang R, Kim S, Chandramouli GV, Barrett JC, Burgoyne PS, Deng CX.** BRCA1, histone H2AX phosphorylation, and male meiotic sex chromosome inactivation. *Curr Biol* 2004; **14**: 2135–2142.
9. **Turner JM, Mahadevaiah SK, Fernandez-Capetillo O, Nussenzweig A, Xu X, Deng CX, Burgoyne PS.** Silencing of unsynapsed meiotic chromosomes in the mouse. *Nat Genet* 2005; **37**: 41–47.
10. **Lee JT.** Sex chromosome inactivation: the importance of pairing. *Curr Biol* 2005; **15**: R249–R252.
11. **Turner JM, Mahadevaiah SK, Ellis PJ, Mitchell MJ, Burgoyne PS.** Pachytene asynapsis drives meiotic sex chromosome inactivation and leads to substantial postmeiotic repression in spermatids. *Dev Cell* 2006; **10**: 521–529.
12. **Hamer G, Novak I, Kouznetsova A, Höög C.** Disruption of pairing and synapsis of chromosomes causes stage-specific apoptosis of male meiotic cells. *Theriogenology* 2008; **69**: 333–339.
13. **Tóth A, Jessberger R.** Male meiosis: Y keep it silenced? *Curr Biol* 2010; **20**: R1022–R1024.
14. **Royo H, Polikiewicz G, Mahadevaiah SK, Prosser H, Mitchell M, Bradley A, de Rooij DG, Burgoyne PS, Turner JM.** Evidence that meiotic sex chromosome inactivation is essential for male fertility. *Curr Biol* 2010; **20**: 2117–2123.
15. **Namekawa SH, Park PJ, Zhang LF, Shima JE, McCarrey JR, Griswold MD, Lee JT.** Postmeiotic sex chromatin in the male germline of mice. *Curr Biol* 2006; **16**: 660–667.
16. **Whyte JJ, Roberts RM, Rosenfeld CS.** Fluorescent in situ hybridization for sex chromosome determination before and after fertilization in mice. *Theriogenology* 2007; **67**: 1022–1031.
17. **Lowe X, O'Hogan S, Moore D 2nd, Bishop J, Wyrobek A.** Aneuploid epididymal sperm detected in chromosomally normal and Robertsonian translocation-bearing mice using a new three-chromosome FISH method. *Chromosoma* 1996; **105**: 204–210.
18. **Wyrobek AJ, Alhborn T, Balhorn R, Stanker L, Pinkel D.** Fluorescence in situ hybridization to Y chromosomes in decondensed human sperm nuclei. *Mol Reprod Dev* 1990; **27**: 200–208.
19. **Egozcue J, Blanco J, Vidal F.** Chromosome studies in human sperm nuclei using fluorescence in-situ hybridization (FISH). *Hum Reprod Update* 1997; **3**: 441–452.
20. **Ko E, Rademaker A, Martin R.** Microwave decondensation and codenaturation: a new methodology to maximize FISH data from donors with very low concentrations of sperm. *Cytogenet Cell Genet* 2001; **95**: 143–145.
21. **Oi M, Yamada K, Hayakawa H, Suzuki H.** Sexing of dog sperm by fluorescence in situ hybridization. *J Reprod Dev* 2013; **59**: 92–96.
22. **Komaki H, Oi M, Suzuki H.** Detection of sex chromosome aneuploidy in dog spermatozoa by triple color fluorescence in situ hybridization. *Theriogenology* 2014; **82**: 652–656.
23. **Kawarasaki T, Sone M, Yoshida M, Bamba K.** Rapid and simultaneous detection of chromosome Y- and 1-bearing porcine spermatozoa by fluorescence in situ hybridization. *Mol Reprod Dev* 1996; **43**: 548–553.
24. **Kobayashi J, Kohsaka T, Sasada H, Umezu M, Sato E.** Fluorescence in situ hybridization with Y chromosome-specific probe in decondensed bovine spermatozoa. *Theriogenology* 1999; **52**: 1043–1054.
25. **Rens W, Yang F, Welch G, Revell S, O'Brien PC, Solanky N, Johnson LA, Ferguson Smith MA.** An X-Y paint set and sperm FISH protocol that can be used for validation of cattle sperm separation procedures. *Reproduction* 2001; **121**: 541–546.
26. **Habermann FA, Winter A, Olsaker I, Reichert P, Fries R.** Validation of sperm sexing in the cattle (Bos taurus) by dual colour fluorescence in situ hybridization. *J Anim Breed Genet* 2005; **122**(Suppl 1): 22–27.
27. **Nicodemo D, Pauciullo A, Castello A, Roldan E, Gomendio M, Cosenza G, Peretti V, Perucatti A, Di Meo GP, Ramunno L, Iannuzzi L, Rubes J, Di Berardino D.** X-Y sperm aneuploidy in 2 cattle (Bos taurus) breeds as determined by dual color fluorescent in situ hybridization (FISH). *Cytogenet Genome Res* 2009; **126**: 217–225.
28. **Bugno M, Jablonska Z, Tischner M, Klukowska-Rötzler J, Pienkowska-Schelling A, Schelling C, Slota E.** Detection of sex chromosome aneuploidy in equine spermatozoa using fluorescence in situ hybridization. *Reprod Domest Anim* 2010; **45**: 1015–1019.
29. **Leblond CP, Clermont Y.** Spermiogenesis of rat, mouse, hamster and guinea pig as revealed by the periodic acid-fuchsin sulfurous acid technique. *Am J Anat* 1952; **90**: 167–215.
30. **Russell LD.** Histological and histopathological evaluation of the testis. 1990.
31. **Hess RA, Renato de Franca L.** Spermatogenesis and cycle of the seminiferous epithelium. *Adv Exp Med Biol* 2008; **636**: 1–15.
32. **Kitajima TS, Ohsugi M, Ellenberg J.** Complete kinetochore tracking reveals error-prone homologous chromosome biorientation in mammalian oocytes. *Cell* 2011; **146**: 568–581.
33. **Kim J, Ishiguro K, Nambu A, Akiyoshi B, Yokobayashi S, Kagami A, Ishiguro T, Pendas AM, Takeda N, Sakakibara Y, Kitajima TS, Tanno Y, Sakuno T, Watanabe Y.** Meikin is a conserved regulator of meiosis-I-specific kinetochore function. *Nature* 2015; **517**: 466–471.
34. **Hecht NB.** Regulation of 'haploid expressed genes' in male germ cells. *J Reprod Fertil* 1990; **88**: 679–693.
35. **Burgoyne PS, Mahadevaiah SK, Turner JM.** The consequences of asynapsis for mammalian meiosis. *Nat Rev Genet* 2009; **10**: 207–216.
36. **Baumgartner A, Schmid TE, Schuetz CG, Adler ID.** Detection of aneuploidy in rodent and human sperm by multicolor FISH after chronic exposure to diazepam. *Mutat Res* 2001; **490**: 11–19.
37. **Attia SM, Badary OA, Hamada FM, Hrabé de Angelis M, Adler ID.** The chemotherapeutic agents nocodazole and amsacrine cause meiotic delay and non-disjunction in spermatocytes of mice. *Mutat Res* 2008; **651**: 105–113.
38. **Attia SM.** Molecular cytogenetic evaluation of the aneugenic effects of teniposide in somatic and germinal cells of male mice. *Mutagenesis* 2012; **27**: 31–39.
39. **Garcia-Quevedo L, Blanco J, Sarrate Z, Vidal F.** Apoptosis mediated by phosphatidylserine externalization in the elimination of aneuploid germ cells during human spermatogenesis. *Andrology* 2014; **2**: 892–898.

Zygote **24** (April), pp. 172–180. © Cambridge University Press 2015
doi:10.1017/S0967199415000027 First Published Online 30 April 2015

Comparison of the effects of BPA and BPAF on oocyte spindle assembly and polar body release in mice

Kei Nakano[2], *Manami Nishio*[2], *Norio Kobayashi*[2], *Yuuki Hiradate*[2], *Yumi Hoshino*[2], *Eimei Sato*[2] *and Kentaro Tanemura*[1]

Laboratory of Animal Reproduction and Development, Graduate School of Agricultural Science, Tohoku University, Sendai, Japan

Date submitted: 01.03.2014. Date revised: 12.12.2014. Date accepted: 25.12.2014

Summary

Bisphenol AF (BPAF), a homolog of bisphenol A (BPA), is a widely used environmental chemical that has adverse effects on reproduction. The aim of this study was to analyse the effects of BPA and BPAF exposure on oocyte maturation *in vitro*. Oocytes were cultured in the presence of BPA or BPAF (2, 20, 50 or 100 μg/ml) for 18 h. At concentrations of 50 and 100 μg/ml, BPA and BPAF inhibited oocyte maturation, with BPAF treatment causing a sharp decrease in the number of oocytes reaching maturity. Oocytes were exposed to BPA or BPAF at 2 μg/ml and cultured for different durations (6, 9, 12, 15 or 18 h). Both BPAF and BPA caused a cell cycle delay under these conditions. Oocytes cultured in the presence of BPA or BPAF (50 μg/ml) for 21 h were tested for the localization of α-tubulin and MAD2 using immunofluorescence. High concentrations of BPAF induced cell cycle arrest through the activation of the spindle assembly checkpoint. After 12 h of culture in BPAF (50 μg/ml), oocytes were transferred to control medium for 9 h. Only 63.3% oocytes treated in this manner progressed to metaphase II (MII). Oocytes exposed to high doses of BPA experienced a cell cycle delay, but managed to progress to MII when the culture period was prolonged. In addition, MAD2 was localized in the cytoplasm of these oocytes. In conclusion, both BPAF and BPA exposure affected oocyte maturation, however BPAF and BPA have differential effects on SAC activity.

Keywords: BPA, BPAF, *In vitro* maturation, MAD2, Oocyte

Introduction

BPA is widely used in the production of polycarbonate plastics and epoxy resins, food packaging, beverage cans, and lacquers for food cans and water pipes. BPA is a xenoestrogen that shares structural features with steroid hormones and modulates the activity of nuclear hormone receptors. Biochemical assays have been used to examine the kinetics of BPA binding to estrogen receptors (ER) and assay results have shown that BPA binds both ERα and ERβ (Gould *et al.*, 1998; Kuiper *et al.*, 1998; Pennie *et al.*, 1998). The affinity of BPA for ERs is 10^4–10^5-fold weaker than that for estradiol. Recently, the estrogen-related receptor γ (ERRγ) was identified as a BPA target receptor. BPA strongly binds to ERRγ and has high constitutive basal activity (Liu *et al.*, 2007; Okada *et al.*, 2008; Takayanagi *et al.*, 2006). In addition, Bouskine *et al.* (2009) reported that, after binding to a membrane G-protein-coupled receptor (GPCR), BPA transmits the extracellular signal through the PKA and PKG pathway to induce a marked increase in JKT-1 cell proliferation (Bouskine *et al.*, 2009).

The exposure of experimental animals to BPA has been shown to have developmental and reproductive effects including increased prostate size, decreased epididymal weight, increased androgen receptor binding activity (Nagel *et al.*, 1997), induction of a uterotrophic response, and reduced estrous cycle

[1]All correspondence to: Kentaro Tanemura. Laboratory of Animal Reproduction and Development, Graduate School of Agricultural Science, Tohoku University, Sendai 981-8555, Japan. Tel:/Fax: +81 22 717 8687. E-mail: kentaro@m.tohoku.ac.jp
[2]Laboratory of Animal Reproduction and Development, Graduate School of Agricultural Science, Tohoku University, Sendai 981–8555, Japan.

(Kim *et al.*, 2001; Laws *et al.*, 2000). Moreover, the treatment of mouse and human oocytes with BPA reportedly has adverse effects on meiotic cell cycle progression, spindle formation, centrosome dynamics, and chromosome alignment and segregation (Can *et al.*, 2005; Lenie *et al.*, 2008).

BPAF is used as an alternative material to BPA for the production of polycarbonate resin (Akahori *et al.*, 2008; Bermudez *et al.*, 2010). BPAF, a homolog of BPA, contains perfluorinated methyl groups and is widely used as a substitute chemical for BPA (Yang *et al.*, 2012). Analysis of the structure–activity relationship of BPA and its related compounds suggests that BPAF is a more dangerous synthetic estrogenic chemical than BPA due to a hydrophobic group substituting for the BPA propane bridge of BPA. This type of substitution has been shown to increase estrogenic activity (Kitamura *et al.*, 2005; Bermudez *et al.*, 2010). *In vitro* studies indicate that BPAF has the ability to bind with both estrogen receptors, ERα and ERβ. The binding affinity of BPAF to ERα and ERβ, respectively, is approximately 20- and 48-fold stronger than that of BPA (Matsushima *et al.*, 2007). Moreover, Matsushima *et al.* (2010) demonstrated that BPAF is a full agonist of ERα, but a highly specific antagonist for ERβ. However, our understanding of the effects of BPAF on development and reproduction is very limited.

Pfeiffer *et al.* (1997) examined the aneuploidogenic potential of BPA and BPAF, in a cell-free system and in V79 cell culture, and demonstrated that both chemicals inhibit microtubule polymerization and increase depolymerisation. Inhibition of microtubule polymerization causes the mis-segregation of chromosomes and can result in the generation of aneuploid embryos with severe birth defects. To ensure faithful chromosome segregation, cells possess a mechanism called the spindle assembly checkpoint (SAC). The SAC is a highly conserved signalling pathway that controls the onset of anaphase, spindle integrity, and corrects chromosome orientation within the spindle (Maney *et al.*, 2000; Hoyt, 2001; Wang & Sun, 2006). Abnormalities in the attachment between kinetochores and kinetochore-associated microtubules activate the SAC, inhibiting the anaphase-promoting complex/cyclosome (APC/C) and arresting cells at the metaphase stage (Maney *et al.*, 2000).

Recent studies have revealed that several mitotic SAC proteins, such as MAD2 (Kallio *et al.*, 2000; Shannon *et al.*, 2002; Wassmann *et al.*, 2003; Zhang *et al.*, 2004; Homer *et al.*, 2005; Ma *et al.*, 2005) also function in meiosis. As a signal transducer in the mitotic checkpoint complex, MAD2 directly binds to cell-division cycle protein 20 (Cdc20) and blocks the activity of APC/C-Cdc20 in a stoichiometric manner (Yu, 2002). MAD2-dependent SAC is functional during the first meiotic division in mouse oocytes (Niault *et al.*, 2007).

Our aim in this study was to elucidate the effects of BPA and BPAF on oocyte maturation by monitoring maturation and MAD2 localization in oocytes cultured using the hanging drop (HD) method.

Materials and Methods

Oocyte collection

Follicle development was stimulated by intraperitoneal injection of 3- to 4-week-old female ICR strain mice (SLC, Shizuoka, Japan) with 5 IU pregnant mare serum gonadotropin (PMSG; Serotropin, Asuka, Tokyo, Japan). Cumulus–oocyte complexes (COCs) were harvested 46–48 h after injection by puncturing large antral follicles with a 26-gauge needle. Retrieved COCs were pooled in Leibovitz's L-15 medium (Invitrogen, Grand Island, NY, USA) containing 0.1% polyvinyl alcohol (PVA; Sigma, St. Louis, MO, USA) and 4 mM hypoxanthine (Sigma) to prevent spontaneous meiotic resumption.

Culture conditions

Obtained COCs were cultured by the HD method of *in vitro* maturation as described previously (Nishio *et al.*, 2014). In this method, a 10-μl droplet of culture medium was deposited in each well of a 96-well plate (Thermo Fisher Scientific) and was overlaid with liquid paraffin (Nacalai Tesque) to prevent contamination and droplet evaporation. A single COC was placed in each droplet, and the plate was inverted and incubated in a humidified atmosphere of 5% CO_2 in air at 37°C. Waymouth's MB 752/1 medium (Invitrogen) was supplemented with 5% fetal calf serum (Sankyo Kagaku, Tokyo, Japan), 0.23 mM pyruvic acid (Nacalai Tesque, Kyoto, Japan), 75 mg/l penicillin G (Meiji Seika, Tokyo, Japan), 50 mg/l streptomycin sulphate (Meiji Seika), 4 mM hypoxanthine (Sigma), 0.1% PVA, and 100 IU/l follicle-stimulating hormone (Sigma). 2, 20, 50 and 100μg/ml BPA or BPAF were added (Wako, Oosaka, Japan) the medium, respectively. BPA or BPAF was dissolved in dimethyl sulphoxide (DMSO), such that the final concentration in the medium was 0.1% (v/v). Four concentrations of BPA or BPAF (2, 20, 50, and 100 μg/ml) were tested. As a control, the medium containing 0.1% DMSO was used.

To assess the concentration-dependent effects on the nucleus maturation rate, COCs were cultured for 18 h. To examine the effects of the cell cycle delay during the maturation, COCs were collected at 6, 9, 12, 15, and 18 h and the nucleus status was examined. To test the effect of 50 μg/ml of BPA and BPAF on the progression of meiosis, COCs were cultured for 18 or 21 h. To

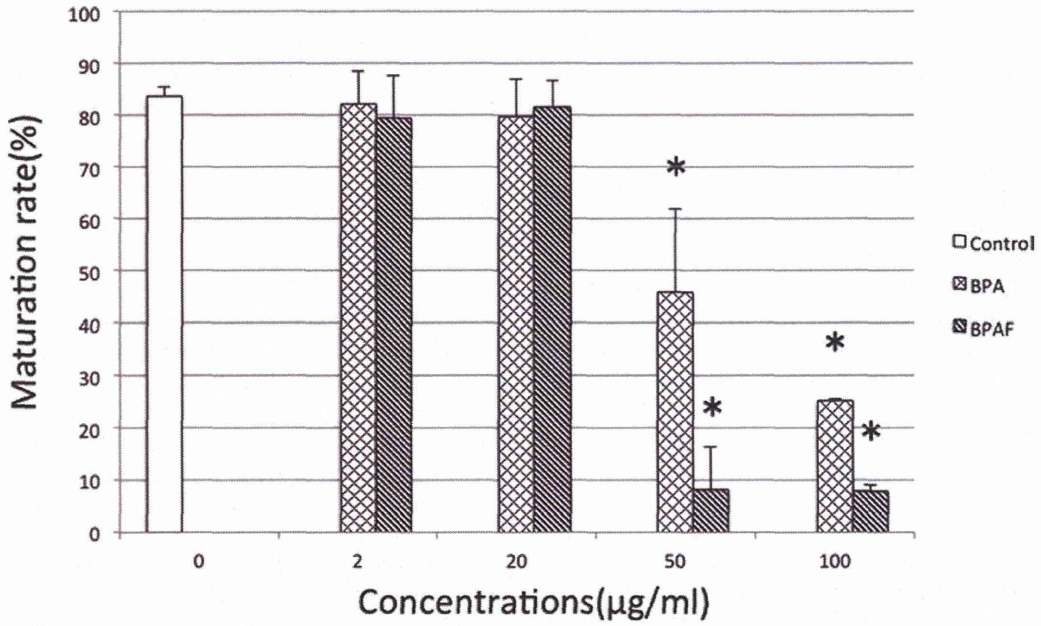

Figure 1 Maturation rate of oocytes exposed to BPA or BPAF at different concentrations. Oocytes were cultured for 18 h. Values are the means ± standard error of the mean (SEM) of three replicates. Bars with different letters are significantly different (*$P < 0.05$).

clarify whether oocytes progress to metaphase II (MII) after BPA or BPAF exposure, COCs were cultured for 12 h in the medium containing 50 μg/ml of BPA or BPAF, followed by 9 h in control medium. Oocyte maturity was evaluated by monitoring first polar body extrusion.

Immunostaining of oocytes

Oocyte immunostaining was performed as described previously (Hoshino and Sato, 2008). Briefly, oocytes exposed to the effective concentration of BPA or BPAF (50 μg/ml) were immunostained with α-tubulin and MAD2 antibodies. Oocytes were denuded from the cumulus cells using 0.1% hyaluronidase (Sigma) and pipetting, fixed at room temperature for 60 min in 2% paraformaldehyde (Sigma) in Dulbecco's phosphate-buffered saline (PBS) without magnesium or calcium PBS (Nissui Pharmaceutical, Ueno, Tokyo, Japan) containing 0.1% PVA and 0.2% Triton X-100 (Wako).

The antibodies used were as follows: rabbit monoclonal anti-MAD2 antibody (Santa Cruz Biotechnology Inc., Santa Cruz, CA, USA; 1:100 dilution); Alexa Fluor 594 donkey anti-rabbit IgG (Molecular Probes, Eugene, Oregano, USA; 1:100 dilution); Alexa Fluor 488 goat anti-mouse IgG (Molecular Probes; 1:100 dilution); and mouse monoclonal anti-α-tubulin (Sigma; 1:200 dilution). Nuclei were labelled using 10 mg/ml Hoechst 33342 (Sigma; 1:100 dilution). Images were acquired using a Zeiss LSM700 confocal microscope.

Statistical analysis

The data were tested statistically using one–way analysis of variance (ANOVA) and Dunnett's test subsequently confirmed homoscedasticity and normality. The analysis software used was SAS 1996 (SAS Institute, USA). Each experiment was repeated three times with at least 30 oocytes. A P-value < 0.05 was considered to be statistically significant.

Results

Effect of BPAF and BPA on oocyte maturation

To analyse the effects of BPA and BPAF on the oocyte maturation, COCs were exposed to 2, 20, 50 or 100 μg/ml BPA and BPAF. Oocytes were cultured for 18 h, the time required to complete oocyte maturation in mice. Compared with controls, cells treated with BPA or BPAF (2 or 20 μg/ml) showed no significant difference in maturity (Fig. 1). However, at concentrations of 50 μg/ml and higher, BPA caused a dose-dependent inhibition of meiotic progress, while BPAF had more potent effects. In the 50 μg/ml BPA-treated group, 45.8% of oocytes reached MII. In comparison, 8.27% of the 50 μg/ml BPAF-treated reached MII. In the groups treated with 100 μg/ml BPA or BPAF, there was also significant decrease in maturation(25.2%, 7.83%).